Hindawi
International Journal of Photoenergy
Volume 2022, Article ID 4912922, 14 pages
https://doi.org/10.1155/2022/4912922

Research Article

Insights into the Enhancement Mechanisms of Molten Salt Nanofluids

Xiong Yaxuan,[1] **Wang Huixiang**,[1] **Wang Zhenyu**,[1] **Wu Yuting**,[2] **Xu Qian**,[3] **Wang Gang**,[1] **Li Chuan**,[2] **Ding Yulong**,[4] **and Ma Chongfang**[2]

[1]*Beijing Key Lab of Heating, Gas Supply, Ventilating and Air Conditioning Engineering, Beijing University of Civil Engineering and Architecture, Beijing 100044, China*
[2]*College of Environmental and Energy Engineering, Beijing University of Technology, Beijing 100124, China*
[3]*School of Energy and Environmental Engineering, University of Science and Technology Beijing, Beijing 100083, China*
[4]*Birmingham Center for Energy Storage, University of Birmingham, Birmingham B15 2TT, UK*

Correspondence should be addressed to Xiong Yaxuan; xiongyaxuan@bucea.edu.cn, Xu Qian; qianxu@ustb.edu.cn, and Li Chuan; lichuan@bjut.edu.cn

Received 13 January 2022; Revised 1 June 2022; Accepted 18 August 2022; Published 13 September 2022

Academic Editor: Daniel T. Cotfas

The addition of nanomaterials to molten salts can significantly improve their thermal performance. To explore the enhancement mechanisms, this work prepared carbonate salt nanofluids with binary carbonate as base salt and 20 nm SiO_2 and 20 nm MgO nanoparticles as additives by the commonly used aqueous solution method. Then, the key performance and micromorphology of the carbonate salt nanofluids are characterized by differential scanning calorimetry, thermal gravimetric analysis, laser flash analysis, and micromorphology analysis. Results showed that the 20 nm SiO_2 nanomaterials instead of the 20 nm MgO nanomaterials exerted higher effects on latent heat while the 20 nm MgO nanomaterials instead of the 20 nm SiO_2 nanomaterials exerted higher effects on the sensible heat, thermal conductivity, and high-temperature stability of carbonated salt. In addition, different nanostructures were observed in SiO_2-based and MgO-based molten salt nanofluids, respectively. Innovatively, formation mechanisms of molten salt nanofluids were proposed based on cloud nuclei to explain the different enhancements in this work.

1. Introduction

As efficient thermal energy storage (TES) materials, molten salt has been widely used in the fields of waste heat recovery, concentrating solar power, and valley power utilization [1, 2]. In recent years, researchers observed that nanomaterials can further improve the TES performance of molten salts and reduce the size of TES systems which will save initial investment cost greatly from investors [3].

In the development process of molten salt nanofluids, Shin and Banerjee conducted the first work and found the anomalous effect of nanomaterials on carbonate salt [3]. In their innovative work [3], Shin and Banerjee added SiO_2 nanoparticles to binary carbonate salt (61.5 mol.% Li_2CO_3-37.5 mol.% K_2CO_3) and found a maximal increase of 24% in specific heat. Moreover, they attributed the anomalous increase to the percolation networks observed in their carbonate salt nanofluid. Later, nanomaterials like SiO_2, MgO, Al_2O_3, SiC, carbon nanotubes (CNTs), graphene, TiO_2, and their mixtures have also been used as additives [4]. Shin and Banerjee [5] added 1.0 wt.% of 10 nm Al_2O_3 nanoparticles to the above binary carbonate salt by the aqueous solution (AS) method, and they obtained that the maximum specific heat increased by about 33% as well as a large number of chain-like nanostructures. Shin and Banerjee [6] prepared carbonate salt nanofluids by dispersing 1.0 wt.% of SiO_2 nanoparticles to the binary carbonate eutectic via the AS method. They observed maximal increases of 14.59% in specific heat and 47% in thermal conductivity, respectively. Shin and Banerjee [7] found high-dense network

substructures in alkali chloride nanofluids with SiO_2 nanoparticles and proposed the three-mode mechanism: (a) the specific heat of nanoparticles is higher than that of the bulk of SiO_2; (b) solid-fluid interaction energy; and (c) liquid molecules are layered on the surface of the nanoparticles, forming a semi-solid layer. Now, the first mode has been confirmed to be not applicable to some molten salt nanofluids. Tiznobaik and Shin [8] found needle-like structures in binary carbonate salt nanofluids with SiO_2 nanoparticles, and they concluded that the high specific surface area of the embedded nanoparticles and the nanoparticle-induced needle-like structures appear to be related to the enhancement of specific heat. Shin and Banerjee [5] considered that the chain-like nanostructures in molten salt nanofluids were responsible for the improvement of specific heat of molten salt nanofluids and that the specific heat can only be improved by the secondary long-range nanostructures formed in carbonate salt nanofluids. Shin and Banerjee [6] attributed the increased thermal conductivity of carbonate salt nanofluids to the observed percolation networks with a higher density phase. Shin et al. [9] considered that a salt component electrostatically interacts with nanoparticles to lead to a microseparation phenomenon of the molten salt mixture, and then, the separated component salt crystallizes on the nanoparticle surface to form the fractal-like fluid nanostructures, which enhance the specific heat of molten salt nanofluids. They also observed the theoretical thermodynamic mixing model [10], thermal conductivity by Hamilton-Crosser model [11], and Maxwell-Garnett model [12] for traditional nanofluids that do not match with the molten salt nanofluids. Rizvi and Shin [4] proposed the theory "development of dendritic structure" to describe the formation of molten salt nanofluids based on theories of the electric double layer and the microsegregation of a binary mixture due to electrostatic interaction and explained how the specific heat of molten salt nanofluids is increased. This theory considers that the dendritic structure on nanoparticles is only one component salt molecule in the molten salt mixture. However, this mechanism is difficult to explain other enhancements like the heat of fusion and the thermal conductivity. Tiznobaik and Shin [13] dispersed 1.0 wt.% of SiO_2 nanoparticles to binary carbonate (62 mol.% lithium carbonate-38 mol.% potassium carbonate) and observed that the specific heat was increased by about 26%. They also concluded that the carbonate salt nanofluids are a mixture of solid nanoparticles, solid nanostructures near nanoparticles, and liquid salt while nanostructures are the cause of increase of specific heat.

Moreover, researchers all over the world are devoted to molten salt nanofluids. Tiznobaik et al. [14] compared the specific heat of the above binary carbonate salt with 1.0 wt.% of different 10 nm nanoparticles, and they observed that the specific heat of MgO, SiO_2, and Al_2O_3 nanoparticles increased by 22%, 27%, and 33%, respectively. Tiznobaik et al. [14] considered that the great specific surface of nanoparticles induced the secondary long-range nanostructures in molten salt nanofluids, and the secondary long-range nanostructures primarily dominated the improvement of specific heat of carbonate salt nanofluids. Jo and Banerjee [15] dispersed 0.1 wt.% of 50 nm graphite nanoparticles to the above binary carbonate and obtained the maximum increase of specific heat of 57%. They also found dense compressed layers on the surface of graphite nanoparticles by scanning electron microscopy (SEM). Jo and Banerjee [16] investigated the effect of multiwalled CNTs on the specific heat of above carbonate salt and found the maximal increases of 15% and 12% in specific heat in liquid and solid state, respectively. Kwak et al. [17] added 2.5 wt.% of SiO_2 nanoparticles to a binary carbonate (62 mol.% lithium carbonate-38 mol.% potassium carbonate) by the AS method, and a maximal increase of 14.59% in specific heat was observed. Based on their research results, Keblinski et al. [18] considered that both the ballistic and the direct or fluid-mediated clustering effects provide a way for rapid heat transport. In addition, they thought that the liquid layer at the liquid/particle interface should be at least several nanometers. Xue et al. [19] found that the thickness of layering of the simple liquid atoms at the liquid-solid interface was several atoms using molecular dynamic simulations and thought that the layering of the simple liquid atoms at the liquid-solid interface did not have any noticeable effect on the heat transport properties. Nevertheless, they also thought that the thickness of the complex liquid atom layering at the liquid-solid interface could extend over longer distances from the interfaces. Oh et al. [20] found the ordered molecule layer at the liquid aluminum/sapphire interface by TEM tests. Using $LiNO_3$ liquid and 10-nm Al_2O_3 nanoparticles, Matthew [21] calculated the thickness of adsorbed layer on the interface. A thickness of 7.1 ± 0.6 nm for enthalpy of fusion and a thickness of 5.3 ± 0.5 nm for specific heat are obtained for 1.0% Al_2O_3 nanoparticles while a thickness of 7.1 ± 0.6 nm for enthalpy of fusion and a thickness of 6.7 ± 0.6 nm for specific heat are obtained for 2.0% Al_2O_3 nanoparticles. This thickness is in the order as what has been reported in literatures [20, 22]. Hentschke [23] argued that the impact of nanoparticles on surrounding liquid was of long range (100 nm or farther) and the formed interfacial mesolayers interacted with each other, which improved the specific heat of molten salt nanofluids. Our recent work [24] found that SiO_2 nanoparticles can also enhance the heat of fusion, specific heat, thermal conductivity, and upper operating temperature of single component salts. Sang and Liu [25] studied the effect of different nanoparticles on a ternary carbonate salt (40 wt.% K_2CO_3-40 wt.% Li_2CO_3-20 wt.% Na_2CO_3), and maximal increases of 116.8%, 73.9%, 56.5%, and 66.5% in specific heat were observed by adding SiO_2, CuO, TiO_2, and Al_2O_3 nanoparticles. Meanwhile, they attributed the increase of specific heat to the dispersion state and quantities of the formed needle-like nanostructures.

It is concluded from the above review that the increased levels in latent heat, specific heat, and thermal conductivity obtained by different researchers are quite different while different microstructures are observed although the nanoparticle, the base salt, and the preparation method employed by these researchers are the same. Therefore, explanations on the enhancement mechanisms of nanoparticles on base salt by different authors are abhorrent.

To explain the enhancement mechanisms of nanoparticles on molten salts, innovatively, this work proposed the formation mechanisms of molten salt nanofluids from the perspective of molecules according to the experimental results in this work and publications and attempted to interpret the mechanism of enhancing the thermal performance of molten salts by adding nanoparticles.

2. Materials and Methods

To provide a basis for the formation mechanisms proposed in Section 3.4, some experiments have been done based on the existing composition of molten salt nanofluid in published literatures.

2.1. Material Preparation. In this work, analytical reagents (Li_2CO_3 and K_2CO_3) were used as component salts to prepare base salt. MgO nanoparticles and SiO_2 nanoparticles were added as additives to prepare carbonate nanofluids, respectively. The purity of the component salts is above 99.0% while the SiO_2 nanoparticles and the MgO nanoparticles were selected with the purity of over 99.8%. MgO and SiO_2 nanoparticles with a mass fraction of 1.0 were dispersed into the base salt (62 mol.% Li_2CO_3-38 mol.% K_2CO_3), respectively. Table 1 shows the specific properties of component salts and nanomaterials.

In this work, the base salt (binary carbonate salt) is prepared with the following steps:

(1) Dried component salts of sodium carbonate and potassium carbonate in a muffle furnace at 300 ˚C for at least 24 h

(2) Weight the dried component salts based on the appropriate mass ratio by an analytical balance (ME 104/02, Mettler Toledo, 0.1 mg) [24], respectively

(3) Ground the component salts in a high-speed disintegrator for 10 s to form a base salt to prepare molten salt nanofluids

(4) Dried the base salt in a drying oven at 170 ˚C for the next preparation process

Molten salt nanofluids containing SiO_2 and MgO nanoparticles are prepared by the AS method, respectively, as described below (Figure 1):

(1) Weighted the base salt and nanoparticles according to preset mass ratio by an analytical balance, respectively

(2) Dispersed different mass ratios of nanoparticles into deionized water at a mass ratio of 1 : 10 and then stirred the solution for 2 h through an ultrasonic agitator to form a homogeneous suspension

(3) Dissolved the base salt into the nanoparticle suspension and stirred until completely dissolved

Table 1: Specific properties of the component carbonates and nanomaterials.

Materials	Purity	Size, nm	T_m, ˚C	ΔH_m, kJ/kg	λ, W/(m·K)	Manufacturer
K_2CO_3	≥99%	—	898	200	1.88	Ref. [26]
Na_2CO_3	≥99%	—	858	280	1.84	
SiO_2	≥99.8%	20	—	—	—	
MgO	≥99.8%	20	—	—	—	

(4) Evaporated the suspension in a vacuum drying oven at 95 ˚C for dehydration to form carbonate salt nanofluid powers

(5) Further dried the carbonate salt nanofluid powers at 170 ˚C for 24 h to ensure complete dehydration of material

Carbonate nanofluids containing SiO_2 nanoparticles are coded as SiO_2-nfs, and carbonate nanofluids containing MgO nanoparticles are coded as MgO-nfs.

To evaluate homogeneity of nanoparticle dispersion in molten salt nanofluids, three samples were taken from three different locations (P1, P2, and P3), as illustrated in Figure 2. For SiO_2-nfs, samples taken from the three locations were coded as samples s11, s12, and s13 while samples taken from the three places were coded as samples s21, s22, and s23 for MgO-nfs.

2.2. Characterization Methods and Uncertainty Analysis. To analyze the dispersion uniformity of nanoparticles in molten salt nanofluids, three samples were taken from different locations of the beaker for every carbonate salt nanofluid. In this work, a synchronous thermal analyzer (STA 449 F3, NETSCH) [24]) was performed to obtain the specific heat, melting point, and heat of fusion of the base salt and molten salt nanofluids using high-purity nitrogen (99.999%) as protective gas and purge gas. Three melting-solidification cycles were carried out at 10 K/min intervals for each sample, and aluminum crucibles were used for the tests. The continuous thermal cycle experiment of the sample is carried out in STA 449 F3, and measurements were repeated seven times for each sample under the same conditions. The sample was heated from 200 to 550 ˚C and then cooled to 200 ˚C in the furnace of the STA 449 F3, during which the heating rate and cooling rate were both 10 K/min.

A laser flasher (LFA 467, NETSCH) was performed to obtain the thermal diffusivity of the base salt and molten salt nanofluids using high-purity nitrogen (99.999%) as protective gas and purge gas, and the thermal conductivity of sample was calculated according to the formula in the literature [27]. Each temperature point was measured seven times, and platinum-rhodium crucibles were used for the tests. Scanning electron microscopy (SEM, SU8000, Hitachi) was performed to observe the micromorphology of base salt and molten salt nanofluids to find potential reasons for the differences in the samples.

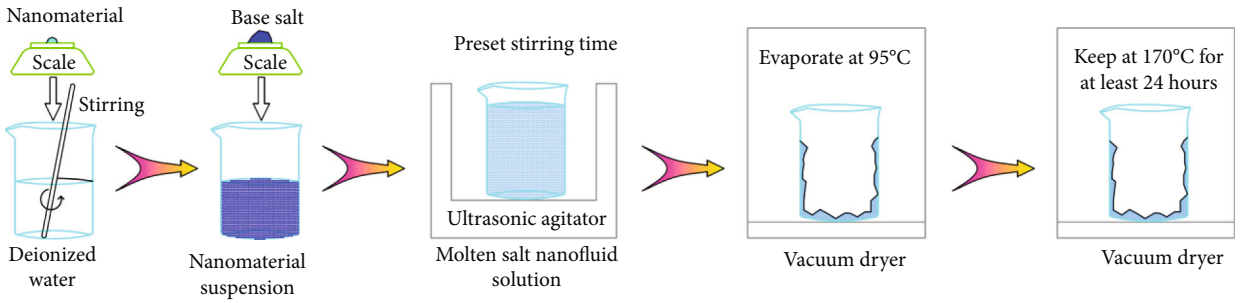

Figure 1: Preparation process of molten salt nanofluids by the AS method.

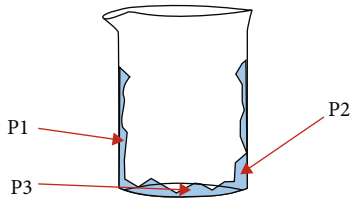

Figure 2: Carbonate nanofluid sampling locations inside the beaker.

The experimental measurement uncertainty was calculated according to the method in the literature [28]; with comprehensive consideration of the standard uncertainty of classes A and B, the measurement uncertainties of the melting point, latent heat, specific heat, and thermal conductivity were calculated to be 0.31 °C, 0.55 J/g, 0.025 J/(g·K), and 0.023 W/(m·K), respectively, in this work.

2.3. Homogeneity and Thermal Stability of Molten Salt Nanofluids

2.3.1. Homogeneity of Nanoparticles. To evaluate the dispersing homogeneity of nanoparticles in carbonate nanofluids, three samples are taken from the three different locations for each nanofluid as described in Section 2.1, and their specific heats are measured, respectively. Table 2 shows the average solid and liquid state specific heats of carbonate nanofluids. In this table, the test results in the first three lines are the average of three cycles.

Table 2 shows that by adding MgO nanoparticles, the average specific heats of the three samples from the three locations are 27.5% and 34.1% higher than those of the base salt in solid state and liquid state, while by adding SiO_2 nanoparticles, the average specific heats of the three samples from different places are only 11.0% and 20.7% higher than those of the base salt in both solid and liquid states. Especially, the standard deviations of the three samples of MgO-nfs are 0.012 J/(g·K) in solid state and 0.054 J/(g·K) in liquid state, while the standard deviations of the three samples of SiO_2-nfs are 0.022 J/(g·K) in solid state and 0.036 J/(g·K) in liquid state. These standard deviations indicate that the dispersion of nanoparticles in the three locations is homogeneous.

2.3.2. Thermal Stability. To investigate the thermal stability of both carbonate nanofluids, the carbonate nanofluid samples were measured repeatedly through ten continuous heating-cooling cycles of 200-560-200 °C. Excluding the phase change process, the average specific heat of carbonate salt nanofluids in solid state and liquid state is shown in Figure 3.

Figure 3 indicates that the average specific heat of both carbonate salt nanofluids keeps generally constant and no obvious variation is found in the specific heats of both carbonate nanofluids after undergoing ten continuous heating-cooling cycles. This indicates that both carbonate nanofluids have excellent thermal stability.

The thermogravimetric curves of both carbonate nanofluids during the heating process are shown in Figure 4. It is observed that the mass losses are 3.49% for MgO-nfs and 4.32% for SiO_2-nfs, respectively, as the carbonate nanofluids are heated up to 1000 °C. The mass loss of base salt is greater than that of both carbonate nanofluids. Obviously, during the heating process, the mass loss of MgO-nfs is less than that of SiO_2-nfs, especially, as the heating temperature is above 800 °C. This indicates that MgO-nfs has better thermal stability than SiO_2-nfs.

3. Results and Discussion

3.1. TES Capacity. To investigate the influence of nanoparticles on the phase change process, the melting point and the latent heat have been measured. Figure 5 depicts the heat flow of the base salt and nanofluids over temperature.

It is clear from Figure 5 that the heat flow curve of SiO_2-nfs moves obviously to the right while the heat flow curve of MgO-nfs keeps nearly unchanged. However, the melting peaks of the base salt are lower than the melting peaks of both nanofluids. Figure 5 indicates that both the MgO nanoparticles and the SiO_2 nanoparticles have an effect on the melting process, but the effects are obviously different.

To verify the equipment, the melting temperature and the latent heat of the base salt were measured and are listed in Table 3, which are consistent with those in refs. [29, 30].

Table 3 indicates the melting temperature and mean latent heat of the carbonate nanofluids. It is observed that the change of the melting point of SiO_2-nfs is significantly smaller than that of MgO-nfs. On the contrary, the increase of the latent heat of SiO_2-nfs is larger than that of MgO-nfs. This confirms the fact again that SiO_2 nanoparticles have little impact on the melting point of molten salts [28].

Table 2: Specific heat of the carbonate salt nanofluids.

Material	Base salt + MgO, J/(g·K)		Base salt + SiO_2, J/(g·K)	
	Solid	Liquid	Solid	Liquid
S11/S21	1.576	2.090	1.378	1.913
S12/S22	1.599	2.141	1.362	1.849
S13/S23	1.586	2.033	1.405	1.908
Average value	1.587	2.088	1.382	1.880
SD	0.012	0.054	0.022	0.036
Increment by	27.5%	34.1%	11.0%	20.7%

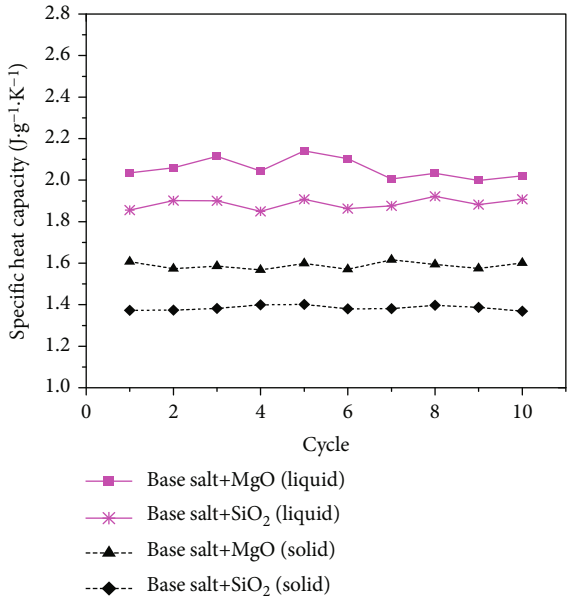

Figure 3: Specific heat of nanofluids after solid-liquid cycles.

Apparently, to increase the TES capacity, the SiO_2-nfs is more beneficial than the MgO-nfs.

In addition, higher specific heat means larger sensible heat to be stored in a TES system. Figure 6 illustrates the specific heat of the base salt, SiO_2-nfs, and MgO-nfs. It is observed that the specific heat of both carbonate nanofluids is all larger than that of the base salt either before or after the phase change. However, the specific heat of MgO-nfs is much higher than that of SiO_2-nfs. This means that the MgO nanoparticles have a greater influence on the sensible heat storage capacity of carbonate nanofluids than that of the SiO_2 nanoparticles. Further, the increases in specific heat of both carbonate nanofluids before the phase change are smaller than those after the phase change, respectively. In addition, the specific heat of both nanofluids increases near linearly over temperature in liquid state.

Figure 6 illustrates that the addition of MgO nanoparticles is superior to the SiO_2 nanoparticles to the binary carbonate for the purpose of sensible heat improvement.

The total TES capacity by the carbonate salt nanofluids consists of the specific heat of the low-temperature ramp-up section, the specific heat of the high-temperature ramp-up section, and the latent heat and the latent heat. Therefore, the total TES capacity can be calculated by equation (1):

$$q_{\mathrm{TES}} = q_{\mathrm{L}} + q_{\mathrm{s,s}} + q_{\mathrm{s,l}}, \tag{1}$$

where

$q_{\mathrm{s,s}} = \int_{T_{\mathrm{init}}}^{T_{\mathrm{melt}}} c_{\mathrm{p,s}} \mathrm{d}T$, $q_{\mathrm{s,l}} = \int_{T_{\mathrm{melt}}}^{T_{\mathrm{max}}} c_{\mathrm{p,l}} \mathrm{d}T$, $q_{\mathrm{L}} = h_{\mathrm{m.}}$

In this work, the initial calculating temperature for TES calculation was 350 °C and the terminal calculating temperature was 550 °C. Figure 7 presents the TES capacity of carbonate nanofluids prepared in this work at different temperatures in the test temperature range.

It is observed that the TES capacity of MgO-nfs increases faster than that of SiO_2-nfs in solid state. This is because the former has higher specific heat than the latter. However, since the latent heat of the MgO-nfs is smaller than that of SiO_2-nfs, the TES capacity of MgO-nfs is close to that of SiO_2-nfs with the termination of the melting process. Further, MgO-nfs also has higher specific heat than SiO_2-nfs in liquid state; therefore, the TES capacity of MgO-nfs increases still faster than that of SiO_2-nfs in the liquid state.

In all, from the point of view of total TES capacity, MgO-nfs are superior to SiO_2-nfs.

3.2. Thermal Conductivity. Thermal conductivity of samples has a decisive influence on heat conduction and convective heat transfer in TES devices, and an improvement in thermal conductivity significantly enhances the heat transfer performance. The thermal conductivity of samples in this work was calculated according to the equations in the literature [27]. The average measured thermal diffusivity of binary carbonate salt is 0.217 mm^2/s. The average thermal diffusivity and the thermal conductivity at different temperatures are illustrated in Figure 8. Obviously, the thermal diffusivities of binary carbonate salt nanofluids are all higher than those of their base salt while the thermal diffusivity of MgO-nfs is higher than that of SiO_2-nfs. Similarly, the thermal conductivities of the binary carbonate salt nanofluids are all far higher than those of their base salt while the thermal conductivity of MgO-nfs is far higher than that of SiO_2-nfs.

Table 4 indicates the detailed values of thermal diffusivity and thermal conductivity. From Table 4, it was observed that the thermal conductivity of MgO-nfs increased by a maximum of 55.7%, which is 26.1% higher than that of SiO_2-nfs. Therefore, MgO-nfs is superior to SiO_2-nfs in terms of heat transfer performance.

3.3. Microscopic Analysis. In Section 2.3, the homogeneity of nanoparticles in molten salt nanofluids has been verified by at least 18 measurements of the specific heat of 6 samples. To determine the micromorphological differences between the two molten salt nanofluids, a SEM was performed to observe the micromorphological of both carbonate nanofluids. The microstructures of binary carbonate salt and carbonate nanofluids are shown in Figure 9.

Figures 9(a) and 9(b) show the microstructure of the base salt at different magnifications. It is observed that the surface of the binary carbonate salt is relatively smooth and dense with an ice-like surface. There is no other special

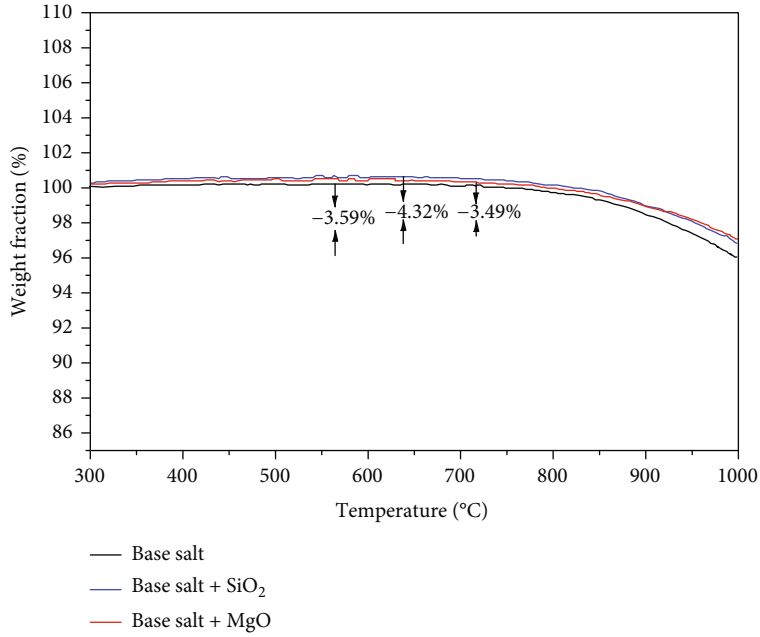

Figure 4: Thermogravimetric curves of the base salt, SiO_2-nfs, and MgO-nfs.

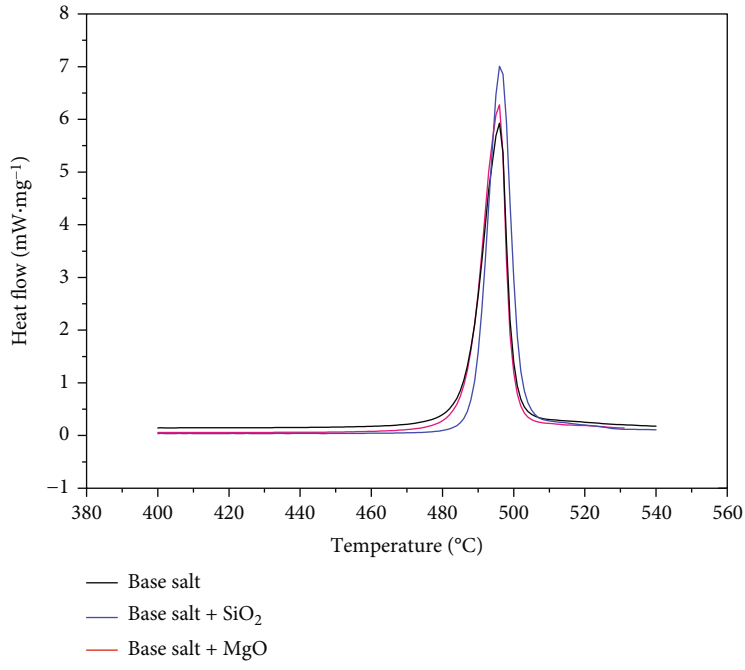

Figure 5: Heat flow of the base salt, SiO_2-nfs, and MgO-nfs.

Table 3: Latent heat and melting temperature of base salt, SiO_2-nfs, and MgO-nfs.

Material	Melting temperature			Latent heat, J/g		
	Avg. value, ˚C	SD	Increase by, ˚C	Avg. value	SD	Increased by, %
Base salt	488.1	0.32	—	351.2	0.64	—
+1.0 wt.% SiO_2 (20 nm)	488.7	0.57	+0.6	381.4	0.8	8.6
+1.0 wt.% MgO (20 nm)	486.9	0.75	−1.2	355.2	0.95	1.1

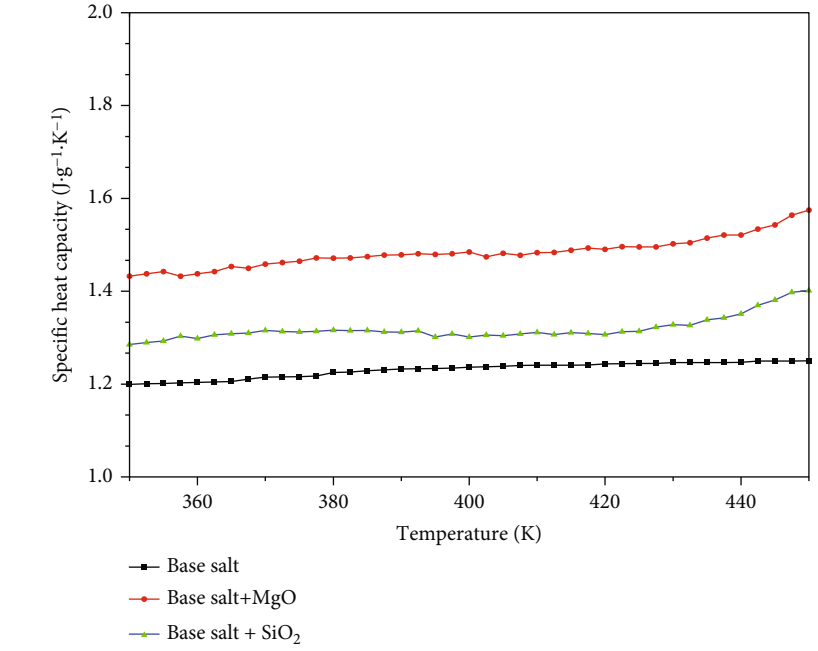

(a) Solid state

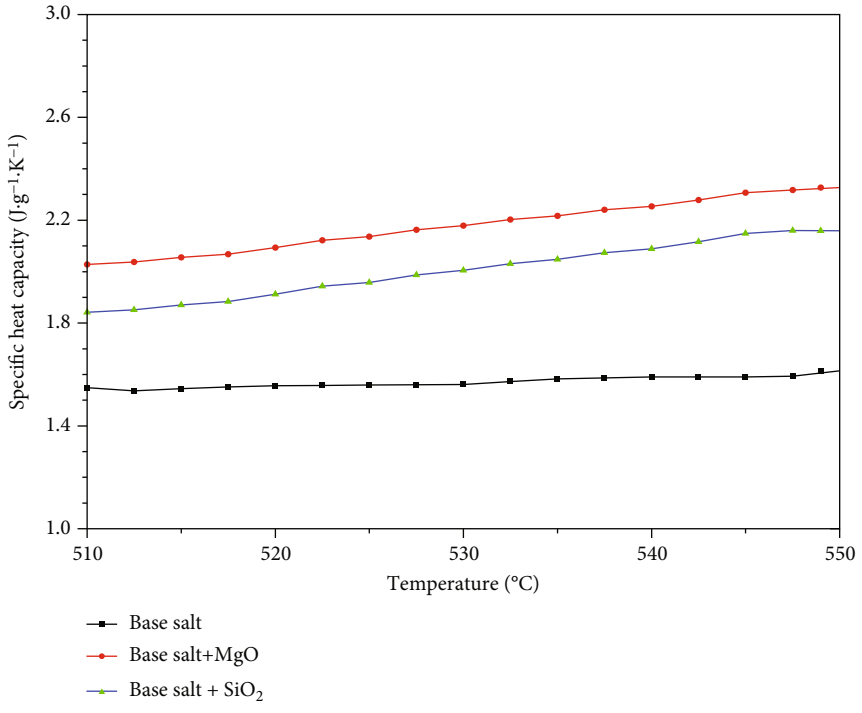

(b) Liquid state

Figure 6: Specific heat of the base slat, SiO_2-nfs, and MgO-nfs.

structure found in the base salt. Figures 9(c) and 9(d) show the microstructure of MgO-nfs. Compared to the binary carbonate salt, massive honeycomb-like crystals are observed. These crystals are almost uniformly distributed. In addition, this carbonate salt nanofluid seems sparse with pore-like structures. Therefore, the specific surface area is increased greatly. It seems that nanoparticles were evenly dispersed in molten salt. Figures 9(e) and 9(f) show the micromorphology of SiO_2-nfs. For this carbonate nanofluid, the microstructure is completely different from the base salt and MgO-nfs. These crystals are with sharp thorns and are covered by the emulsion-like substance, which seems to be raised stalactite. Moreover, these crystals are evenly distributed. Obviously, the specific surface area of this molten salt

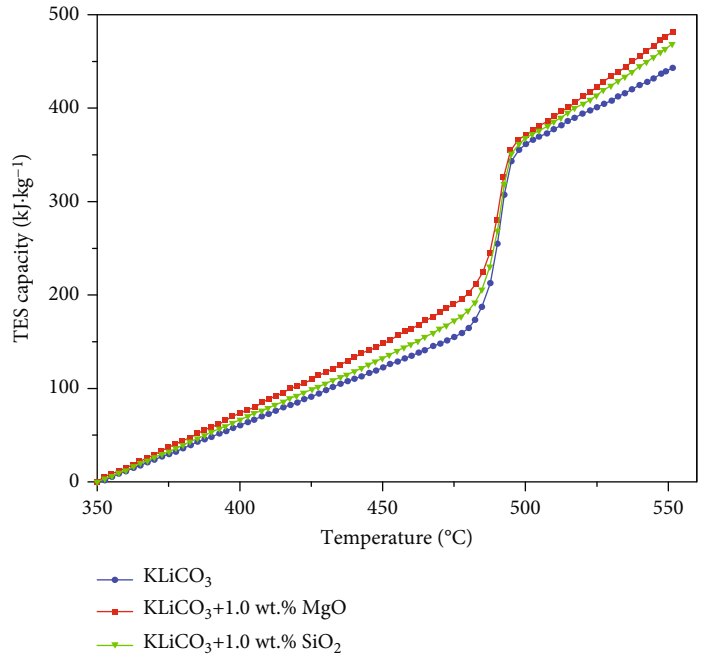

Figure 7: TES capacity of base salt, SiO_2-nfs, and MgO-nfs variates over temperature.

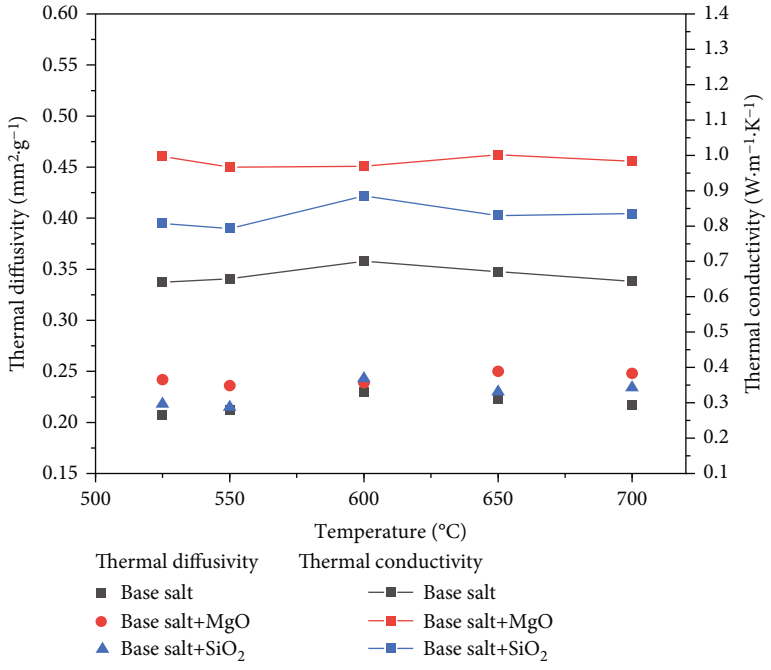

Figure 8: Thermal diffusivity and thermal conductivity of base salt, SiO_2-nfs, and MgO-nfs variates over temperatures.

nanofluid is between the base salt and MgO-nfs. In addition, it is found that no obvious agglomeration of nanoparticles is observed in both carbonate nanofluids.

3.4. Mechanisms of Formation and Performance Enhancement. The above results show that both types of nanoparticles have significant but different impacts on the thermal performance and the micromorphology of base salt. However, how do the molten salt nanofluids form? What is the mechanism of enhancement?

3.4.1. Formation of Molten Salt Nanofluid. As nanoparticle size approaches atom size, atom density on the nanoparticle surface is very high. Therefore, there are a lot of free bonds

Table 4: Thermal conductivity and thermal diffusivity of base salt, SiO_2-nfs, and MgO-nfs.

Material		525 °C	550 °C	600 °C	650 °C	700 °C
Base salt	α (mm^2/s)	0.207	0.212	0.230	0.223	0.217
	λ (W/(m·K))	0.641	0.651	0.700	0.671	0.644
MgO-nfs	α (mm^2/s)	0.242	0.236	0.239	0.250	0.248
	λ (W/(m·K))	0.997	0.967	0.969	1.002	0.983
	Enhancement (%)	55.7	48.6	38.4	49.3	52.5
SiO_2-nfs	α (mm^2/s)	0.218	0.215	0.243	0.230	0.234
	λ (W/(m·K))	0.807	0.793	0.885	0.830	0.835
	Enhancement (%)	26.0	21.9	26.4	23.7	29.6

connecting free atoms which lack coordination atoms. This causes the nanoparticles to have high unsaturation, high chemical activity, high specific surface energy, and strong hydrophilicity. Therefore, nanoparticles can easily interact with water and form hydroxyl groups on their surface.

According to the AS method presented in Section 2.1, nanoparticles (as illustrated in Figure 10(a)) firstly are dispersed into deionized water by ultrasonic agitation.

As nanoparticles meet water molecules, free atoms on nanoparticle surface will split water molecules into -OH groups and -H atoms to fill unsaturated free bonds and form the first layer, namely, the hydroxyl group layer, on the nanoparticle surface (from Figure 10(b)). Meanwhile, the ultrasonic agitation accelerates the formation of hydroxyl groups. This layer is also depicted by the green annulus in Figures 10(d)–10(f).

SiO_2 nanoparticles with amorphous space structure have irregular Si-O tetrahedral branched network. As can be seen from Figure 10(c), hydroxyl groups with space distance less than 3 Å in a nanoparticle and between adjacent nanoparticles will interact with each other to form hydrogen bonds while water molecules will also interact with isolated hydroxyls and pair hydroxyls on nanoparticle surface to form additional hydrogen bonds with the increase of mixing time. However, for MgO nanoparticles, the free atoms and the formed hydroxyl groups are equal in the pace distance, which is more than 3 Å. Therefore, there are no hydrogen bonds formed by adjacent hydroxyl groups on the same nanoparticle. This is one of the main differences between SiO_2 nanoparticles and MgO nanoparticles during the interaction with water molecules. Moreover, during the ultrasonic agitation process, the soft-agglomerated nanoparticle clusters will break up into individual nanoparticles and smaller nanoparticle clusters, while some individual nanoparticles will collide with each other and form hard-agglomerated nanoparticle clusters with different sizes. They also form hydroxyl groups and then hydrogen bonds on the surface of hard nanoparticle clusters. At this stage, the interaction flux between nanoparticles and water molecules reduces to zero while the nanoparticle surface is full of water molecules connected by hydrogen bonds.

As we know, it is not easy for molten salt ions to interact with hydrogen bonds on nanoparticle surface. As base salts are added, under the interaction of Van der Waals between nanoparticle and molten salt ions and the electrostatic force between hydrogen bonds and molten salt ions, the molten salt ions move closer to the nanoparticle surface, as illustrated in Figure 10(e). Figure 10(e) shows that the molten salt ions are adsorbed to the nanoparticle surface layer by layer to form cloud nuclei. Massive cloud nuclei, centered with nanoparticles and surrounded by molten salt ions, form in molten salt nanofluid until the interaction between the outermost molten salt ions and surrounding nanoparticles reaches a dynamic thermodynamic equilibrium [24]. However, more potassium ions will be adsorbed by the centered nanoparticles due to their larger zeta potential. Therefore, the ratio of potassium ions to sodium ions in cloud nuclei is larger than that in the base salt, which has been verified by the literature [4]. These cloud nuclei suspend in salt-water solution which appears translucent. During the mixing process, insufficient agitation time cannot produce the maximum number of cloud nuclei and some nanoparticles may not form saturated cloud nuclei while too long agitation would destroy some cloud nuclei and cause some cloud nuclei to agglomerate hardly.

In engineering applications, to produce molten salt nanofluid for convenient transportation, water must be evaporated completely. During this process, the molten salt nanofluid will crystallize and the solid cloud nuclei will form as the water evaporates completely. Before molten salt nanofluids are charged into the TES tanks, the molten salt nanofluids have to be melted into liquid at first.

As mentioned above, molten salt ions located at the edge of cloud nuclei are in dynamic equilibrium. When the temperature of the molten salt nanofluid rises to its terminal melting temperature, the molten salt ions located outside the cloud nuclei melt completely. With a further increase of the molten salt nanofluid temperature, molten salt ions inside the cloud nuclei gradually lose their dynamic equilibrium and melt starting from the edge to the center of the cloud nuclei. As the temperature of molten salt nanofluid rises to some level above the melting point, the molten salt ions adsorbed by Van der Waals force inside the cloud nuclei melt completely. At this time, water molecules are still adsorbed by the hydrogen bonds between hydroxyl groups and water molecules and the Van der Waals force between the nanoparticle and water molecules. Therefore, water molecules are still difficult to leave the nanoparticle surface. When the temperature of molten salt nanofluid rises to a higher level, the hydrogen bonds start to break. As the

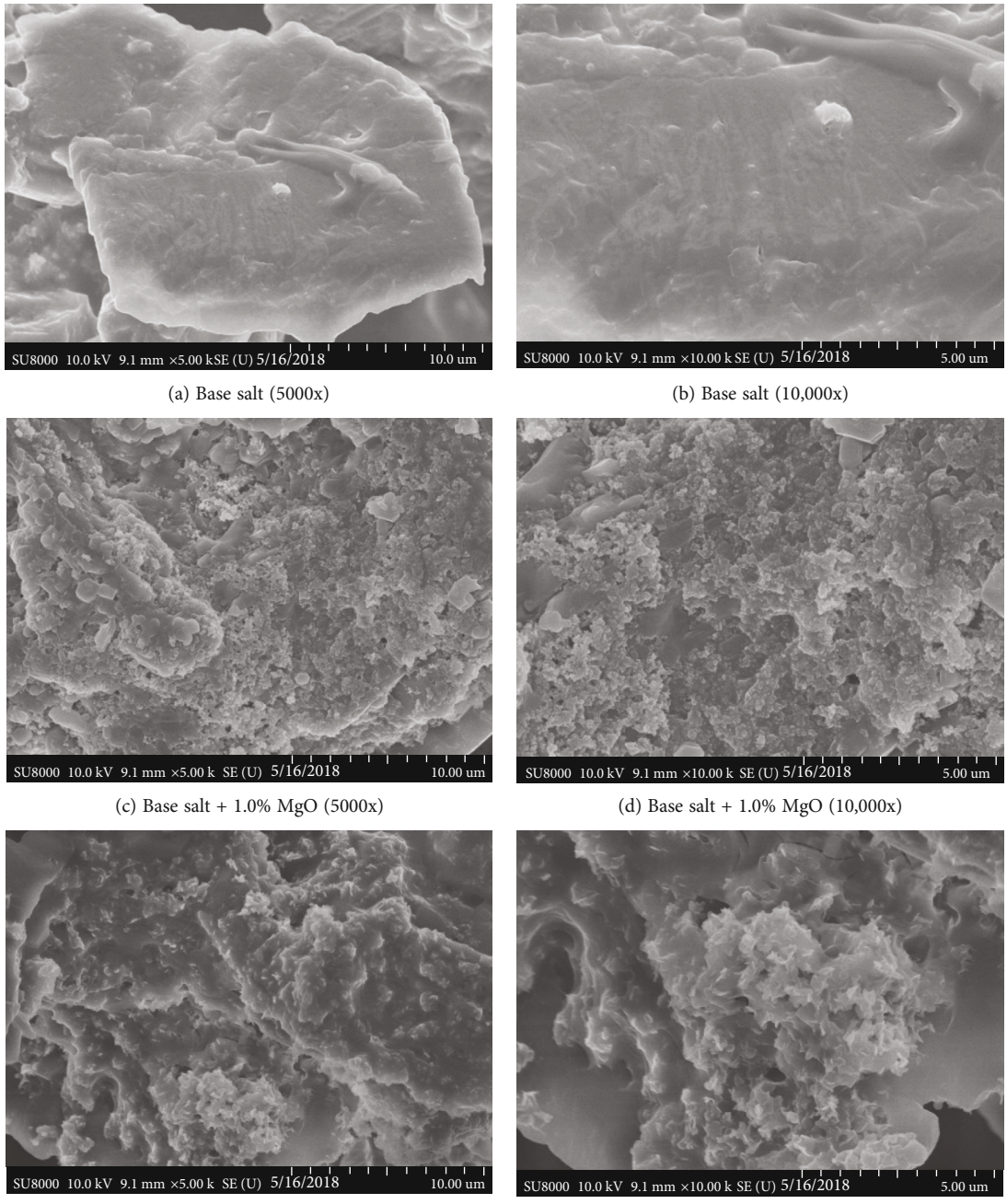

(a) Base salt (5000x)

(b) Base salt (10,000x)

(c) Base salt + 1.0% MgO (5000x)

(d) Base salt + 1.0% MgO (10,000x)

(e) Base salt + 1.0% SiO_2 (5000x)

(f) Base salt + 1.0% SiO_2 (10,000x)

Figure 9: Micromorphology of the base salt, SiO_2-nfs, and MgO-nfs.

hydrogen bonds inside the cloud nuclei are broken, the adsorbed water molecules will leave the cloud nuclei and evaporate from molten salt nanofluid while hydroxyl groups will form again on the nanoparticle surface. However, as the temperature for hydroxyl groups to leave the nanoparticle is far higher than the operating temperature of the molten salt nanofluid, hydroxyl groups will keep being adsorbed on the nanoparticle surface. Therefore, the cloud nuclei in the molten salt nanofluid prepared by the AS method consist of three parts: the centered nanoparticle, the hydroxyl groups (middle layer), and the molten salt (outer layer), as illustrated in Figure 11.

The other difference between the SiO_2 nanoparticles and the MgO nanoparticles is that both types of nanoparticles have completely different physicochemical properties. Therefore, the cloud nuclei that they formed in their molten salt nanofluids are completely different in size and structure. This also leads to the difference of cloud nuclei in micromorphology in SiO_2-nfs and MgO-nfs.

3.4.2. Enhancement of Specific Heat. The carbonate nanofluids are prepared to undergo some melting/high-temperature-heating/solidification cooling cycles. Through the above experiments, the authors observed that the specific heat of

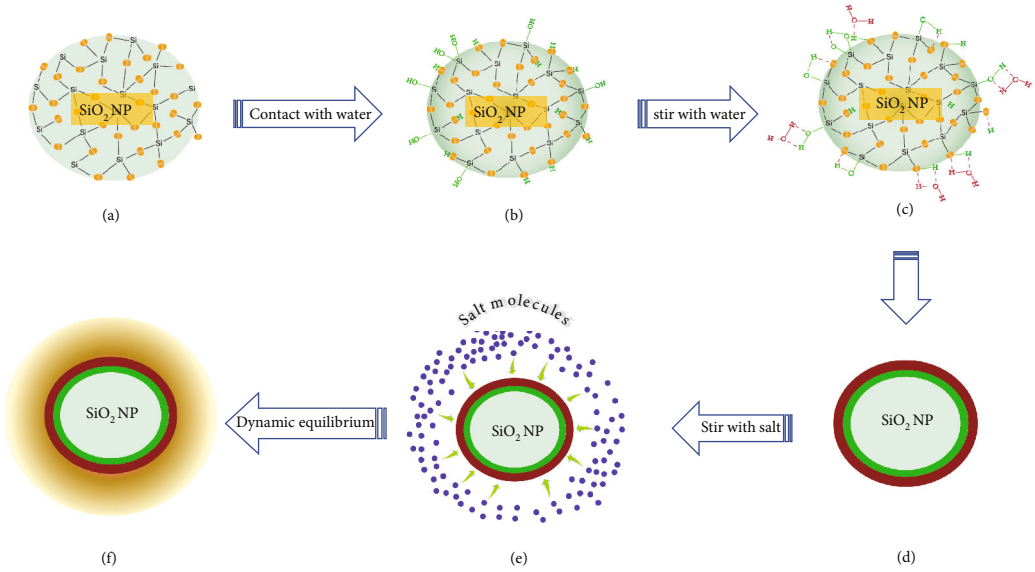

Figure 10: Formation mechanism of molten salt nanofluids prepared by AS method. (a) SiO_2 nanoparticle. (b) SiO_2 nanoparticle with hydroxyl groups. (c) SiO_2 nanoparticle with hydroxyl groups and water molecules. (d) Thumbnail of Figure 10(c). (e) Molten salt ions move toward nanoparticle. (f) Formed cloud nucleus with three attached layers.

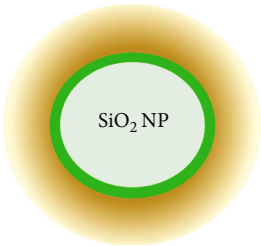

Figure 11: Structure of cloud nuclei in the molten salt nanofluid by the AS method after a high-temperature heating/solidification cycle.

the carbonate nanofluids increased abnormally. Based on the formation mechanisms proposed in Section 3.4.1, the anomalous increase in the specific heat can be explained as follows.

After the bulk salt melts completely with the temperature increase of bulk salt, the salt inside the cloud nuclei starts to melt gradually from the edge to the inside of the cloud nuclei due to the total interaction between the centered nanoparticle and the molten salt ions inside the cloud nuclei that is larger than that between the centered nanoparticle and the bulk molten salt ions outside the cloud nuclei. In addition, with the reduction of distance between the centered nanoparticle and the molten salt ions inside the cloud nuclei, the total interaction between the centered nanoparticle and the molten salt ions inside the cloud nuclei increases rapidly.

As we know, when the temperature rises up to some level, the molten salt nanofluid system will reach a new molecular dynamic equilibrium. With the further increase of bulk nanofluid temperature, the distance between nanoparticles and molten salt ions inside the cloud nuclei will become larger and larger. Then, molten salt ions will leave the cloud nuclei and the diameter of cloud nuclei will be smaller and smaller, as illustrated in Figure 12, which is consistent with the layer-by-layer desorption scenario [21]. During this process, much more heat is needed, which explains why the specific heat of molten salt nanofluid increases. Otherwise, more heat will be released during the overall temperature reduction. Due to the formation of the cloud core structure, the specific heat of carbonate nanofluids prepared by the aqueous solution method increases sharply after layer-by-layer analysis, with an increase of ~121.85% [31].

3.4.3. Enhancement of Heat of Fusion. Undeniably, when the molten salt nanofluid system reaches some molecular dynamic equilibrium, the centered nanoparticles interact not only with molten salt ions inside the cloud nucleus but also with those molten salt ions in the bulk salt. The main difference between the molten salt ions inside the cloud nuclei and the bulk molten salt ions is that molten salt ions in both fields are in different molecular dynamic equilibria. Once pure thermal energy is input into the molten salt nanofluid system, the equilibria will be broken and new equilibria tend to form. Therefore, the melting of bulk molten salt has to overcome the interaction force between nanoparticles and bulk molten salt ions. At this moment, some more thermal energy has to be supplied. This means that the latent heat of molten salt nanofluid increases. However, because the interaction force between nanoparticles and bulk molten salt ions is very weak, this increase of the heat of fusion is very small. The review shows that the latent heat increases by 33% when different nanoparticles are added to binary carbonate [14]. The increase in latent heat is much smaller compared to the increase in specific heat.

3.4.4. Enhancement of Thermal Conductivity. As can easily be imagined, there is an interaction force between different

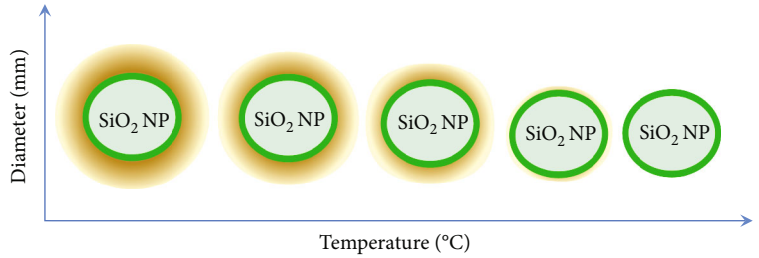

Figure 12: Diameter change of cloud nuclei over temperature.

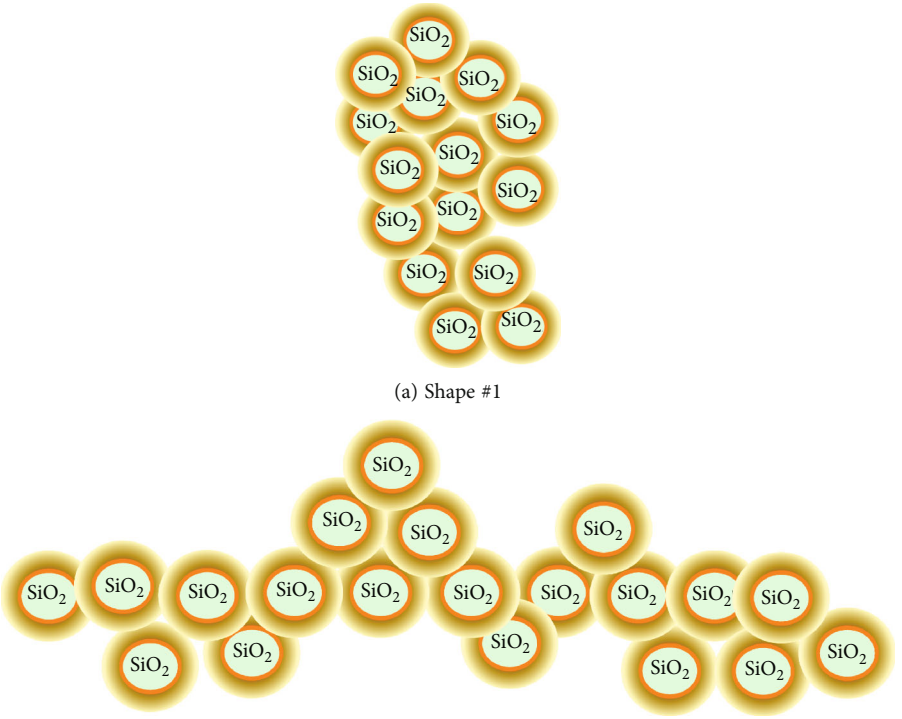

(a) Shape #1

(b) Shape #2

Figure 13: Diameter change of cloud nuclei over temperature.

cloud nuclei. This interaction force will cause some adjacent cloud nuclei to approach and form different shapes of chains made up of cloud nuclei, as illustrated in Figure 13. These chains are very small relative to the great volume of the carbonate salt nanofluid, and therefore, the distribution of these chains in the carbonate salt nanofluid is random.

According to the ballistics in nanoparticles and the direct or fluid-mediated clustering effects [18], phonons can transport heat through nanoparticles and cloud nuclei and finally transport through the chains of cloud nuclei rapidly. Therefore, the thermal diffusivity and the thermal conductivity of carbonate salt nanofluids are increased greatly.

However, because the cloud nuclei formed in SiO_2-nfs are different from those formed in MgO-nfs, the increased levels of both carbonate salt nanofluids are different. In addition, different mixing times, different evaporation containers, ratio of water to nanoparticles, and other factors will form different cloud nuclei in size and structure, which will cause the different increase levels of carbonate salt nanofluids. It indicated that the addition of nanoparticles (SiO_2 and carbon nanotubes) to carbonate increased the thermal conductivity by 50% [32]. The increase in thermal conductivity is also different with the addition of different nanoparticles.

3.4.5. Effect on Microstructure. As we know, SiO_2 is an atom crystal while magnesia is an ionic crystal. Also, as mentioned above, SiO_2 nanoparticles with an amorphous space structure have an irregular Si-O tetrahedral branched network while MgO nanoparticles have a regular space structure. In addition, both the SiO_2 nanoparticles and the MgO nanoparticles have different physicochemical properties. Therefore, the cloud nuclei in both molten salt nanofluids have different sizes and different crystal structures though structures of the cloud nuclei in both molten salt nanofluids look similar. The difference in structure inevitably leads to the

difference in micromorphology of SiO_2-nfs and MgO-nfs. This is also sure for molten salt nanofluids with the same type but different concentrations of nanoparticles by different mixing times. Though the base salt and nanoparticles are the same, the cloud nuclei also have different sizes and different structures in these molten salt nanofluids, which are caused by the different mixing time and other factors.

4. Conclusions

This work innovatively proposed the formation mechanisms of molten salt nanofluids based on a molecular perspective, and the formation mechanisms were used to explain the enhancement mechanisms of nanomaterials on carbonate salt based on experimental data obtained in this work. Some conclusions are made as follows:

(1) Specific heat is improved by maximal 20.7% and 34.1% by SiO_2 and MgO nanoparticles while the thermal conductivity is increased by maximal 29.6% and 55.7%, respectively. The high-temperature stability of MgO-nfs is better than that of SiO_2-nfs while the two types of molten salt nanofluids have excellent homogenization

(2) Different nanostructures have been observed in SiO_2-nfs and MgO-nfs, which are formed because of the different sizes and structures of cloud nuclei and led to the different enhancement of their thermal energy storage performance

(3) Cloud nuclei formed in the molten salt nanofluid during the preparation process by the AS method, which is made of four parts: the centered nanoparticle, the hydroxyl groups (middle layer), the water molecules, and the molten salt (outer layer). After a high-temperature heating/solidification cycle, the cloud nuclei are simplified into three parts: the centered nanoparticle, the hydroxyl groups (middle layer), and the molten salt (outer layer). These cloud nuclei are different due to the different nanomaterials, mixing time, and some other factors

(4) Interaction between nanoparticles and bulk molten salt enhances the heat of fusion while the process of molten salt molecules leaving or approaching the cloud nuclei enhances the specific heat of molten salt nanofluids and the chains of cloud nuclei enhance the thermal conductivity of molten salt nanofluids

4.1. Future Work. In the following work, we will further investigate homogenization after a long-time static placement and fluid flow. More detailed formation mechanisms will be explored and analyzed further.

Data Availability

This article includes all the data used to support the research results. If necessary, you can contact the author to provide data.

Conflicts of Interest

The author declares that this article is published without any conflict of interest.

Acknowledgments

The authors are grateful to the financial support of the Scientific Research Program of Beijing Municipal Education Commission under Project (Grant No. KM201910016011), the National Nature Science Foundation of China under Project (Grant No. 51206004), and the Beijing Municipal Natural Science Foundation (3151001).

References

[1] M. Aneke and M. Wang, "Energy storage technologies and real life applications—a state of the art review," *Applied Energy*, vol. 179, pp. 350–377, 2016.

[2] Q. Yu, Z. Jiang, L. Cong et al., "A novel low-temperature fabrication approach of composite phase change materials for high temperature thermal energy storage," *Applied Energy*, vol. 237, pp. 367–377, 2019.

[3] D. Shin and D. Banerjee, "Enhanced specific heat of silica nanofluid," *Journal of Heat Transfer*, vol. 133, no. 2, article 024501, 2011.

[4] S. M. M. Rizvi and D. Shin, "Mechanism of heat capacity enhancement in molten salt nanofluids," *International Journal of Heat and Mass Transfer*, vol. 161, article 120260, 2020.

[5] D. Shin and D. Banerjee, "Specific heat of nanofluids synthesized by dispersing alumina nanoparticles in alkali salt eutectic," *International Journal of Heat and Mass Transfer*, vol. 74, pp. 210–214, 2014.

[6] D. Shin and D. Banerjee, "Enhanced thermal properties of SiO_2 nanocomposite for solar thermal energy storage applications," *International Journal of Heat and Mass Transfer*, vol. 84, pp. 898–902, 2015.

[7] D. Shin and D. Banerjee, "Enhancement of specific heat capacity of high-temperature silica-nanofluids synthesized in alkali chloride salt eutectics for solar thermal-energy storage applications," *International Journal of Heat and Mass Transfer*, vol. 54, no. 5-6, pp. 1064–1070, 2011.

[8] H. Tiznobaik and D. Shin, "Enhanced specific heat capacity of high-temperature molten salt-based nanofluids," *International Journal of Heat and Mass Transfer*, vol. 57, no. 2, pp. 542–548, 2013.

[9] D. Shin, H. Tiznobaik, and D. Banerjee, "Specific heat mechanism of molten salt nanofluids," *Applied Physics Letters*, vol. 104, no. 12, article 121914, 2014.

[10] J. Buongiorno, "Convective transport in nanofluids," *ASME Journal of Heat Transfer*, vol. 128, no. 3, pp. 240–250, 2006.

[11] R. Hamilton and O. Crosser, "Thermal conductivity of heterogeneous twocomponent systems," *Industrial & Engineering Chemistry Fundamentals*, vol. 1, no. 3, pp. 187–191, 1962.

[12] C. Nan, R. Birringer, D. Clarke, and H. Gleiter, "Effective thermal conductivity of particulate composites with interfacial thermal resistance," *Journal of Applied Physics*, vol. 81, no. 10, pp. 6692–6699, 1997.

[13] H. Tiznobaik and D. Shin, "Experimental validation of enhanced heat capacity of ionic liquid-based nanomaterial," *Applied Physics Letters*, vol. 102, no. 17, article 173906, 2013.

[14] H. Tiznobaik, D. Banerjee, and D. Shin, "Effect of formation of "long range" secondary dendritic nanostructures in molten salt nanofluids on the values of specific heat capacity," *International Journal of Heat and Mass Transfer*, vol. 91, pp. 342–346, 2015.

[15] B. Jo and D. Banerjee, "Enhanced specific heat capacity of molten salt-based nanomaterials: effects of nanoparticle dispersion and solvent material," *Acta Materialia*, vol. 75, pp. 80–91, 2014.

[16] B. Jo and D. Banerjee, "Enhanced specific heat capacity of molten salt-based carbon nanotubes nanomaterials," *Journal of Heat Transfer*, vol. 137, no. 9, article 091013, 2015.

[17] H. E. Kwak, D. Shin, and D. Banerjee, "Enhanced sensible heat capacity of molten salt and conventional heat transfer fluid based nanofluid for solar TES application," in *ASME 2010 4th International Conference on Energy Sustainability*, vol. 2, pp. 735–739, Phoenix, Arizona, USA, 2010.

[18] P. Keblinski, S. R. Phillpot, S. U. S. Choi, and J. A. Eastman, "Mechanisms of heat flow in suspensions of nano-sized particles (nanofluids)," *International Journal of Heat and Mass Transfer*, vol. 45, no. 4, pp. 855–863, 2002.

[19] L. Xue, P. Keblinski, S. R. Phillpot, S. U. S. Choi, and J. A. Eastman, "Effect of liquid layering at the liquid-solid interface on thermal transport," *International Journal of Heat and Mass Transfer*, vol. 47, no. 19-20, pp. 4277–4284, 2004.

[20] S. Oh, Y. Kauffmann, C. Scheu, W. Kaplan, and M. Ruhle, "Ordered liquid aluminum at the interface with sapphire," *Science*, vol. 310, no. 5748, pp. 661–663, 2005.

[21] W. Matthew, *Adsorption at the nanoparticle interface for increased thermal capacity in solar thermal systems*, MIT, Cambridge, Massachusetts, 2012.

[22] W. Kaplan and Y. Kauffmann, "Structural order in liquids induced by interfaces with crystals," *Annual Review of Materials Research*, vol. 36, no. 1, pp. 1–48, 2006.

[23] R. Hentschke, "On the specific heat capacity enhancement in nanofluids," *Nanoscale Research Letters*, vol. 11, no. 1, p. 88, 2016.

[24] Y. Xiong, Z. Wang, M. Sun et al., "Enhanced thermal energy storage of nitrate salts by silica nanoparticles for concentrating solar power," *International Journal of Energy Research*, vol. 45, no. 4, pp. 5248–5262, 2021.

[25] L. Sang and T. Liu, "The enhanced specific heat capacity of ternary carbonates nanofluids with different nanoparticles," *Solar Energy Materials and Solar Cells*, vol. 169, pp. 297–303, 2017.

[26] Y. Xiong, M. Sun, Y. Wu et al., "Effects of synthesis methods on thermal performance of nitrate salt nanofluids for concentrating solar power," *Energy & Fuels*, vol. 34, no. 9, pp. 11606–11619, 2020.

[27] Y. Xiong, C. Song, J. Ren et al., "Sludge-incinerated ash based shape-stable phase change composites for heavy metal fixation and building thermal energy storage," *Process Safety and Environmental Protection*, vol. 162, pp. 346–356, 2022.

[28] Y. Xiong, Z. Wang, Y. Wu et al., "Performance enhancement of bromide salt by nano-particle dispersion for high- temperature heat pipes in concentrated solar power plants," *Applied Energy*, vol. 237, pp. 171–179, 2019.

[29] Y. Tao, C. Lin, and Y. He, "Preparation and thermal properties characterization of carbonate salt/carbon nanomaterial composite phase change material," *Energy Conversion and Management*, vol. 97, pp. 103–110, 2015.

[30] M. Kenisarin, "High-temperature phase change materials for thermal energy storage," *Renewable and Sustainable Energy Reviews*, vol. 14, no. 3, pp. 955–970, 2010.

[31] B. Jo and D. Banerjee, "Effect of solvent on specific heat capacity enhancement of binary molten salt- based carbon nanotube nanomaterials for thermal energy storage," *International Journal of Thermal Sciences*, vol. 98, pp. 219–227, 2015.

[32] L. Sang, W. Ai, Y. Wu, and C. Ma, "SiO_2-ternary carbonate nanofluids prepared by mechanical mixing at high temperature: enhanced specific heat capacity and thermal conductivity," *Solar Energy Materials and Solar Cells*, vol. 203, article 110193, 2019.